Chitosan nanocomposite hydrogel and scaffold for controlled drug delivery

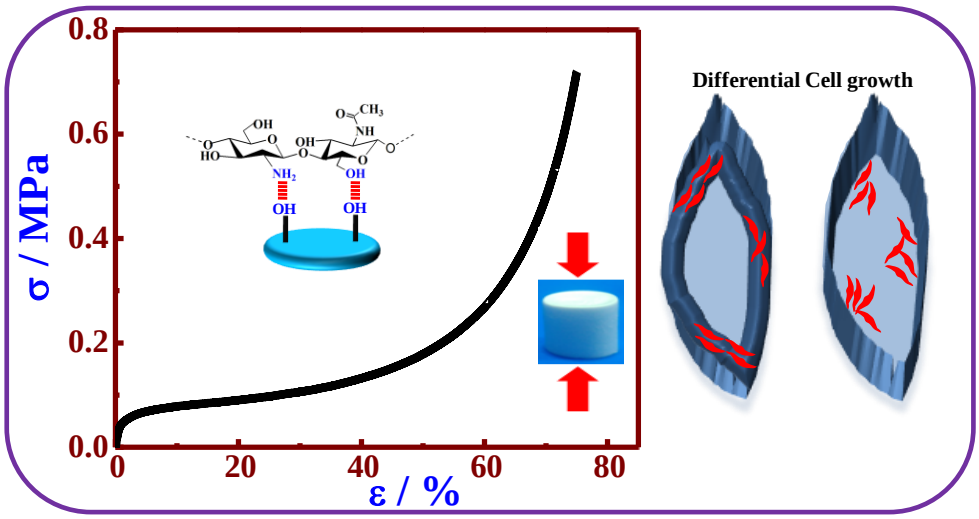

5.1 Introduction

Now days, Controlled drug delivery technology is one of the most rapidly growing areas of science in which chemist and chemical engineers are contributing to human health care [Feng et al., 2010; Xu et al., 2010; Manna et al., 2010; Fatouros et al., 2014; Zhao et al., 2015]. Controlled drug delivery systems have various advantages over conventional dosages forms. Both synthetic and natural polymers are extensively used for control drug delivery systems [Hoffman et al., 2002]. Natural polymers have greater priority over the synthetic polymers because of biocompatible and nontoxic nature. Natural polymer, either protein (collagen, gelatin and albumin) or polysaccharide (starch, dextran, hyaluronic acid, pectin and chitosan) are used for drug delivery system [Gupta et al., 2012; Naira et al., 2007]. Among different natural polymers studied, Chitosan is of great interest because of its biocompatibility, biodegradability, nontoxicity, and mucoadhesive properties. Chitosan, Poly(*β*-(1→4)-2-amino-2-deoxy-D-glucose) is the deacetylated derivative of chitin, is used for different applications including food, regenerative engineering, cosmetics [Kim et al., 2005; Jiang et al., 2014; Wang et al., 2011; Thein-Han et al., 2009; Malafaya et al., 2009]. Chitosan has great contribution in drug delivery applications because of its well-documented biocompatibility and biodegradability [Muzzarelli et al., 2007; Mahanta et al., 2015; Liu et al., 2008; Mahanta et al., 2016; Wang et al., 2016].

Chitosan has low mechanical strength which is great drawbacks which restrict its use in wide range of application. Nanocomposite technology has been introduced to cope up with this situation. Nanofillers such as carbon nanotubes, clay and hydroxyapatite and graphene oxide have been used to enhance the different properties of chitosan [19-22]. The mechanical strength of chitosan can be enhanced with homogeneous dispersion of nanofiller in chitosan matrix.

In this chapter, we have report innovative chitosan nanohybrids with sufficient mechanical strength for controlled drug delivery and tissue engineering purpose. Chitosan nanohybrids hydrogel and scaffold have been prepared with two types of nanofillers of opposite surface charge (-Ve for 30B and +ve for LDH). The structure and the morphology of the hydrogel of pure CHT and its nanohybrids are evaluated. The effects of extensive interaction of nanofillers with the CHT matrix on mechanical properties are investigated. Tunable sustained drug delivery can be achieved with the nanohybrids. The biocompatibility natures of the nanohybrids are checked with the NIH 3T3 mouse embryonic fibroblast cells. The developed nanohybrids hydrogel and scaffold of CHT have the potential to be used as controlled drug delivery and tissue engineering.

5.2 Results and discussion:

5.2.1 Extent of dispersion and interaction in nanohybrids

Chitosan nanohybrids have been developed using two different types of nanofillers (30B and LDH, respectively). Homogeneous dispersion of nanofillers is observed in nanohybrids by the bright field TEM image (**Figure 5.1a**). Homogeneously dispersed hexagonally-shape LDH plates are clearly observed in CHT-L, whereas intercalated structure is observed for CHT-C. The spectroscopic techniques are used to understand the relative interaction in nanohybrids as results of good dispersion of nanofillers. The FTIR spectra of pure chitosan and its nanohybrids are shown in **Figure 5.1b**. The characteristics peaks of CHT are observed at 3218 $cm^{-1}$for the amine and hydroxyl groups; the absorption band at 1633 cm^{-1} is for the carbonyl (>C=O) stretching of the secondary amide, the bending vibrations of the >N-H are observed at 1571 cm^{-1}[Nanda et al., 2011; Kim et al., 2013]. The broad band at 3218 cm-1 for CHT is shifted to the

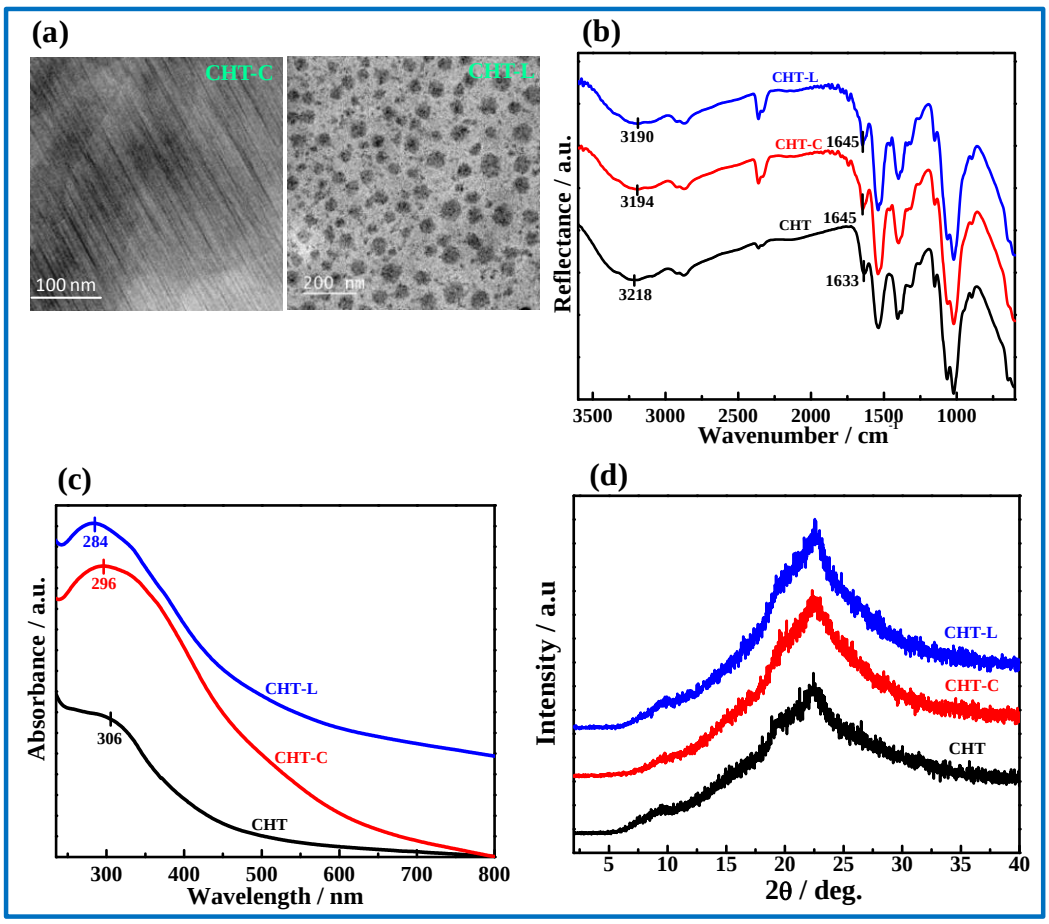

Figure 5.1: (a) TEM image of indicated nanohybrids; (b) FTIR spectra of pristine CHT and its corresponding nanohybrids; Vertical lines indicate the peak positions; (c) UV-visible spectra of pristine chitosan and its corresponding nanohybrids. Inset figure shows the absorption spectra of pure PU; (d) XRD pattern of pure CHT and its indicated nanohybrids.

lower frequency in nanohybrids indicating interaction of the nanofiller with the CHT molecules. The greater shifting in CHT-L (3190cm^{-1}) compared to the CHT-C (3194cm^{-1}) strongly indicates that the nature of interaction is much greater in CHT-L compared to CHT-C. The shifting of amide I band to 1645 cm^{-1} from 1645 cm^{-1}in nanohybrids also suggests good interaction of CHT and nanofillers. UV-visible measurements also confirm the interaction between CHT and nanofillers (**Figure 5.1c**). Pure CHT shows n→π* absorption at 306 nm which shifted to lower wavelength in nanohybrids at 284 and 296

nm for CHT-C and CHT-L, respectively. Higher shifting in CHT-L indicates stronger the interaction between CHT and LDH compared to CHT and 30B. The X-ray diffraction pattern of pure CHT and its corresponding nanohybrids has been shown in **Figure 5.1d**. In pure chitosan, two peaks are observed at 9.2 and 22.4^{o} for hydrated crystalline and amorphous structure, respectively [Mahanta et al., 2017; Wang et al., 2005]. Nanofillers don't affect the crystallinity nature of the pure polymer as evident from the peak position remain unchanged in the nanohybrids.

5.2.2Morphology and the mechanical response

Figure 5.2a represents the SEM images of cross-sectional scaffolds of pure CHT and its corresponding nanohybrids. Highly porous morphology is observed for the scaffolds. Nanohybrid scaffolds show a more uniform porous structure. The hydrophilic nature of pure chitosan is significantly changed in presence of nanofiller, while CHT-L is more hydrophilic and CHT-C is hydrophobic (**Figure 5.2b**). The deswelling profile also shown in **Figure 5.2c**. Solvent retention ability of the hydrogels is almost the same (**Figure 5.2d**).

Hydrogel and Scaffold should have sufficient mechanical strength to with stand in vivo mechanical stress while providing support to the ingrowing tissue for tissue engineering purpose. The mechanical property of lyophilized hydrogel scaffold was determined from the uniaxial compression technique shown in **Figure 5.3a**. All the nanohybrids show higher modulus in compared to pure CHT. Nanoclay (30B) incorporated nanohybrid (CHT-C) exhibits a 26% improvement of the modulus, while dramatic enhancement (187%) is observed for LDH based nanohybrid incompared to pure CHT (**Figure 5.3b**). Homogeneously distributed LDH nanoparticle in CHT matrix

exerts greater interaction with the CHT matrix as observeved in FTIR, correlating the huge increment of the modulus of CHTL, while enhancement in modulus of CHT-C

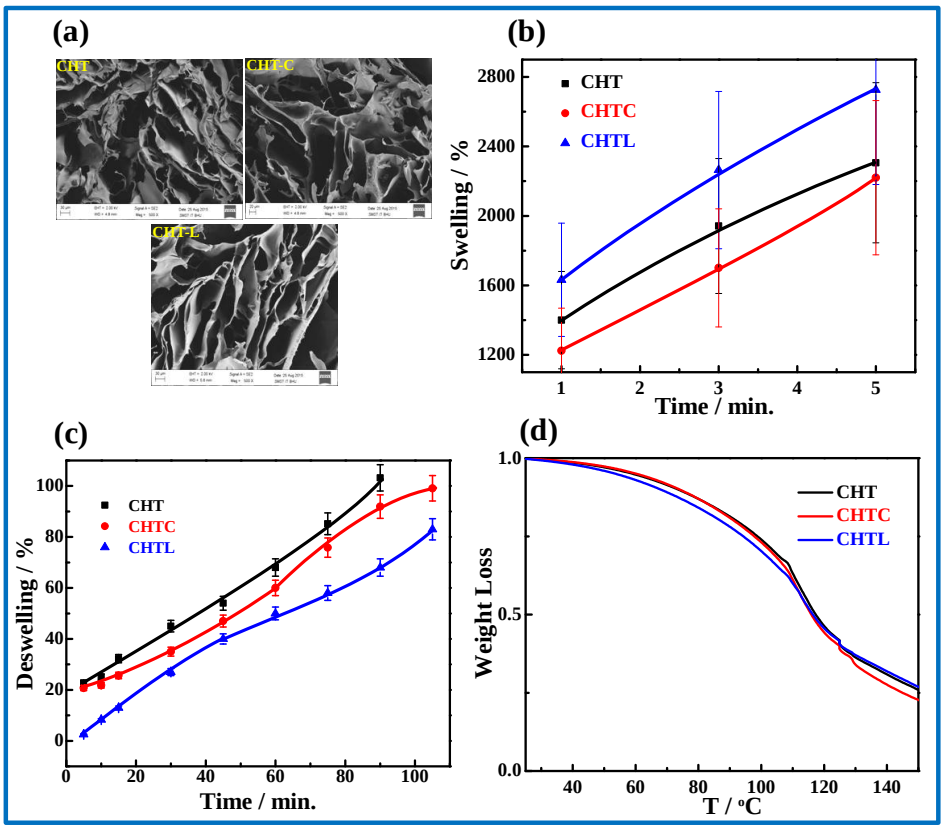

Figure 5.2: (a) SEM image of lyophilized hydrogel of pristine CHT and its indicated nanohybrids; (b) Swelling kinetics of pure CHT and its indicated nanohybrids. (c) Deswelling profile of pure CHT and its nanohybrids. (d) Solvent retention property of the hydrogel of pure CHT and its indicated nanohybrids.

is attributed to the intercalated structure where polymer chains are sandwiched within the nanoclay gallery showing higher elasticity [Singh et al., 2012]. The toughness of pure CHT and its corresponding nanohybrid are measured from the area under the stress-strain curves shown in **Figure 5.3c**. Measured toughness are 14, 9 and 11 MJm^{-3} for CHT-L, CHT-C, and Pure CHT, respectively. Dynamic rheological experiments were performed as a function of frequency to understand the hydrogel strength of pure CHT and its nanohybrids. The frequency dependence storage modulus, loss modulus, and complex

viscosity, in dynamic mode were measured at 30 °C and have been shown in **Figure 5.4a**.

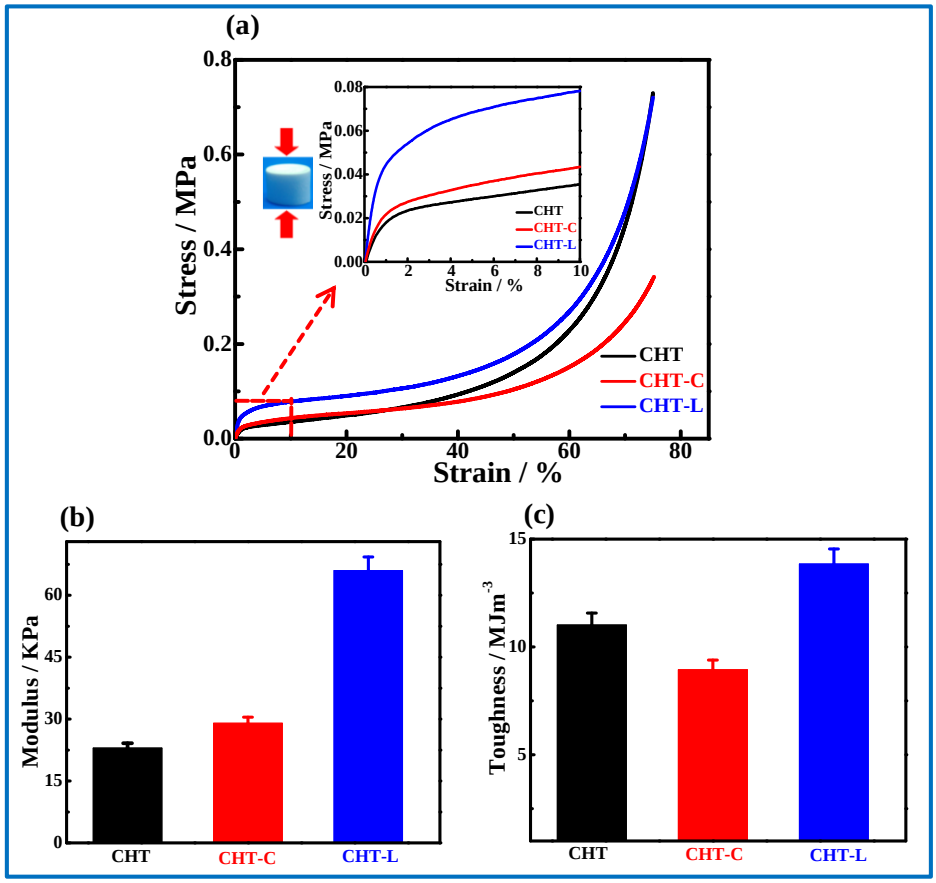

Figure 5.3: (a) Stress-Strain curves of the scaffold of pure CHT and its corresponding nanohybrids, modulus and toughness are showing in figure (b) and (c), respectively.

The storage modulus of all the nanohybrids increases as compared to pure CHT and the order is same as found in stress-strain behavior. η* (ω) also exhibits the same behavior as observed in storage modulus. Higher gel strength for the nanohybrids is attributed to the hydrogen bonding between the nanofiller and pure chitosan and nature of the interaction is in the order of CHT-L > CHT-C. The shear viscosity in the steady state measurement is shown in **Figure 5.4b**.

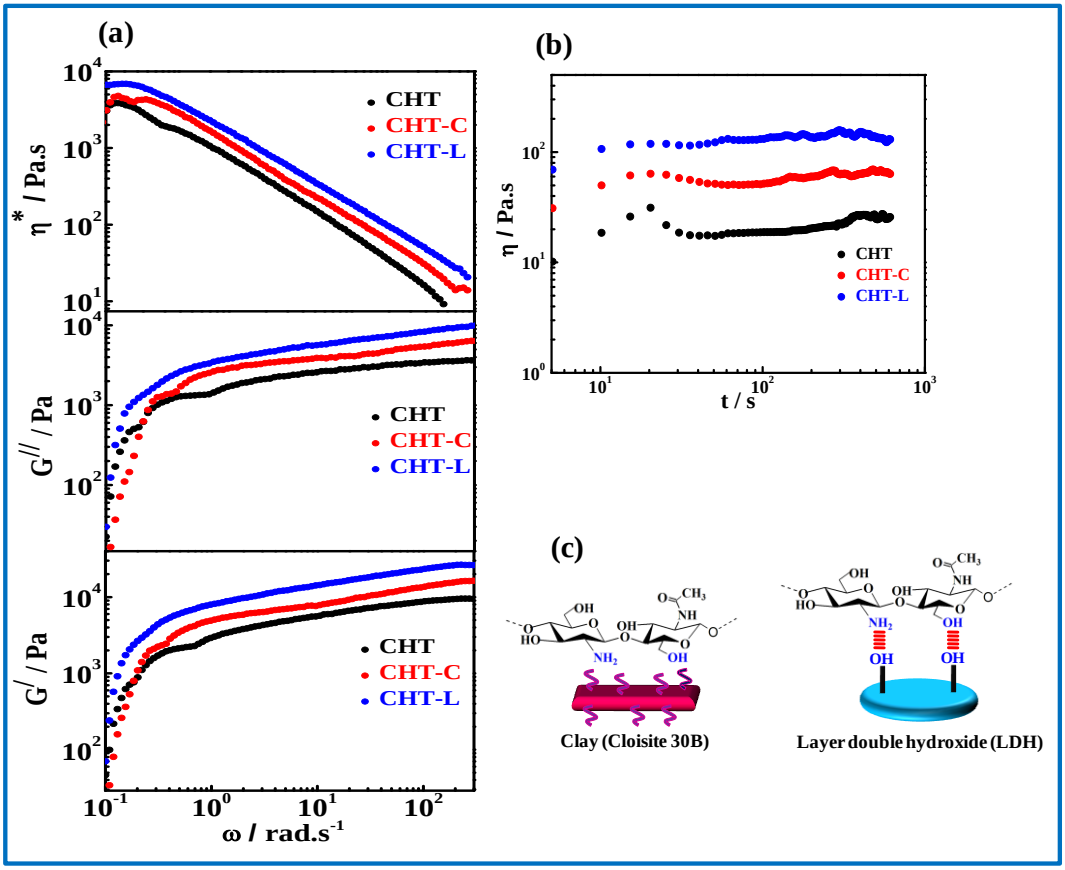

Figure 5.4: (a) Mechanical Response of the hydrogel of CHT and its corresponding nanohybrids in dynamic mode, bottom storage modulus ($G^{/}$), middle loss modulus ($G^{//}$) and top viscosity (η∗); (b) Steady shear viscosity (η) Vs. time of hydrogel of CHT and its corresponding nanohybrids; (c) Schematic model showing interaction between different nanofiller with pure polymer matrix (CHT).

The viscosity of nanohybrid gel exhibits the higher viscosity in comparison to pure chitosan indicating similar nature as observed dynamic behavior and the viscosity remains constant over a long period of time. Greater interaction in nanohybrids is the reinforcement for enhancing the mechanical strength of the nanohybrids as compared to the pure chitosan in both hydrogel and scaffold. CHT-L shows greater interaction because of extensive hydrogen bonding with chitosan molecules while CHT-C shows interaction through dipolar interaction schematically shown in **Figure 5.4c**.

5.2.3 Sustained drug delivery

The controlled drug delivery systems are designed in such a way that can provide an alternative approach to regulating the bioavailability of the therapeutic agents. Nanohybrids hydrogel and scaffold of chitosan have been designed to control the release kinetics for better therapeutic efficacy of the given drug. *In vitro,* drug release assays are carried out with the drug loaded hydrogel and scaffold in PBS (pH~7.4) at 37 ^{o}C maintaining the physiological condition. Tetracycline hydrochloride, an antibacterial drug is used as a model drug to understand the in vitro release behavior. The cumulative percent release as a function of time is shown in **Figure 5.5a and b**, respectively. Hydrogels and scaffolds exhibit sustained release kinetics as compared to pure chitosan. Drug release kinetics from the scaffold is found faster than using hydrogel. Scaffolds exhibit 90, 69, and 56% of drug release at 15 hours from CHT, CHT-C, and CHT-L, respectively, while it is 74, 54, and 44% at 48 hours using hydrogel of the said specimen. Hydrogels show more sustained drug release behavior as compared to the scaffolds over a long period of time. Slow drug release behavior of nanohybrids also can be visualized from the antibacterial activity tested against Gram-negative bacteria *E. coli*. Formation of the zone of inhibition for drug embedded nanohybrids is less than drug embedded chitosan which is good agreement with the in vitro drug release pattern (**Figure 5.5d**). The observed Zone of inhibitions are 2.9, 2.6 and 2.2 cm forCHTDG, CHT-CDG and CHT-LDG hydrogels respectively. There are couples of steps which controlled the drug release phenomena from the polymer network; liquid penetration into the matrix, dissolution of the drug and diffusion of the drug from the drug embedded matrix [Patel et al., 2016]. In vitro, drug release kinetics are fitted with different kinetic model to understand the release kinetics and the mechanism of the drug release (**Table 5.1a and**

b). Korsmeyer-Peppas model is found to be best fitted. Korsmeyer-Peppas model is obtained from the two equations (a and b) [Dash et al., 2010].

$\frac{M_t}{M_\infty} = Kt^n$ …….. (a)

Which in logarithmic form is

$\log\frac{M_t}{M_\infty} = \log K + n\log t$ ……... (b)

where$M_t/M_\infty$is the fraction of drug released at time t, n is the diffusion, K is the rate constant exponent. The value of 'n' indicates the nature of diffusion mechanism of the drug where n ≤ 0.45 corresponds to a Fickian diffusion mechanism and 0.45 < n < 0.89 represents non-Fickian diffusion mechanism.

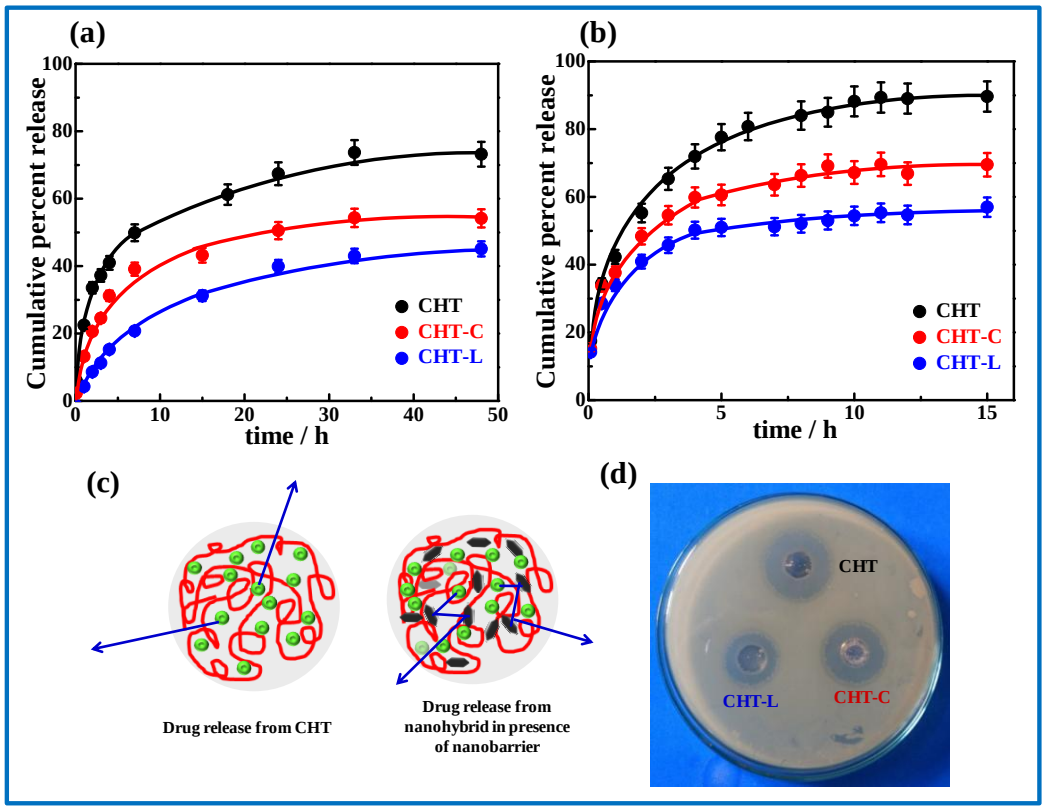

Figure 5.5: *In vitro* Drug release profile for pure CHT and its indicated nanohybrids: (a) using hydrogel and (b) Scaffold. (c) Schematic model illustrating drug release from CHT and its corresponding nanohybrids; (d) Digital photograph of antibacterial activity using drug loaded hydrogel of pure CHT and its indicated nanohybrids.

It is worthy to mention that the pure chitosan in both cases (hydrogel and scaffold) exhibit Fickian nature of drug diffusion (n < 0.45). Nanohybrids show a different type of diffusion nature in hydrogel and scaffold. Scaffolds show Fickian nature of drug diffusion (n <0.45) while hydrogels of nanohybrids show non-Fickian nature of drug diffusion (n > 0.45).

Table 5.1: In vitro drug release kinetics were fitted with different mathematical model and the obtained Release rate constant (*k*), correlation coefficient (r_2) and diffusion release exponent (*n*) are given in (a) and (b) using hydrogel and scaffold, respectively for pure CHT and its indicated nanohybrids.

(a)

Sample	Zero Order		First Order		Higuchi		Korsmeyer-Peppas	
	K	r^2	*K*	r^2	*K*	r^2	*n*	r^2
CHT	6.35 ± 0.65	0.79	0.051 ± 0.015	0.84	12.04 ±2.54	0.88	0.40 ± 0.003	0.98
CHT-C	3.45 ± 0.45	0.88	0.043 ± 0.011	0.77	7.82 ±2.25	0.77	0.46 ± 0.006	0.99
CHT-L	2.54 ± 0.32	0.83	0.036 ± 0.005	0.71	8.11 ± 1.40	0.75	0.53 ± 0.008	0.98

(b)

Sample	Zero Order		First Order		Higuchi		Korsmeyer-Peppas	
	K	r^2	*K*	r^2	*K*	r^2	*n*	r^2
CHT	10.75 ± 0.87	0.91	0.077 ± 0.005	0.90	32.71 ±1.01	0.77	0.42 ± 0.004	0.99
CHT-C	8.37 ± 0.63	0.87	0.063 ± 0.006	0.77	18.49 ± 0.6	0.89	0.38 ± 0.005	0.99
CHT-L	6.52 ± 0.59	0.77	0.054 ± 0.002	0.71	15.54 ±0.77	0.71	0.34 ± 0.002	0.99

The interaction of the drug molecules with the matrix also play an important role in drug release occurring from the polymeric network through diffusion nature. The interaction of the drug molecules with the matrix has been studied through FTIR and UV-visible

measurement. The FTIR spectra of pure samples (CHT and CHT-C) and their corresponding drug loaded specimen (CHTDG and CHT-CDG) along with the pure drug (DG) has been shown in the **Figure 5.6a**. The absorption band corresponding to the O-H and N-H vibration has been shifted to the higher wavenumber in presence of drug. The shifting is found to be higher in nanohybrids than chitosan indicating greater interaction of the drug molecules with the nanohybrids. Amide I band also shifted to the lower wavenumber in presence of the drug and the shifting is higher for nanohybrid. The interaction of the drug molecules with the matrix also clearly observe through UV-visible studies (**Figure 5.6b**). The well-known characteristics peaks of the drug molecule is observed at 277 and 358 nm for $\pi \rightarrow \pi *$ and $n \rightarrow \pi *$, respectively shown in inset figure of **Figure 3f** [Ghadim et al., 2013]. These peaks are shifted to lower wavelength in drug

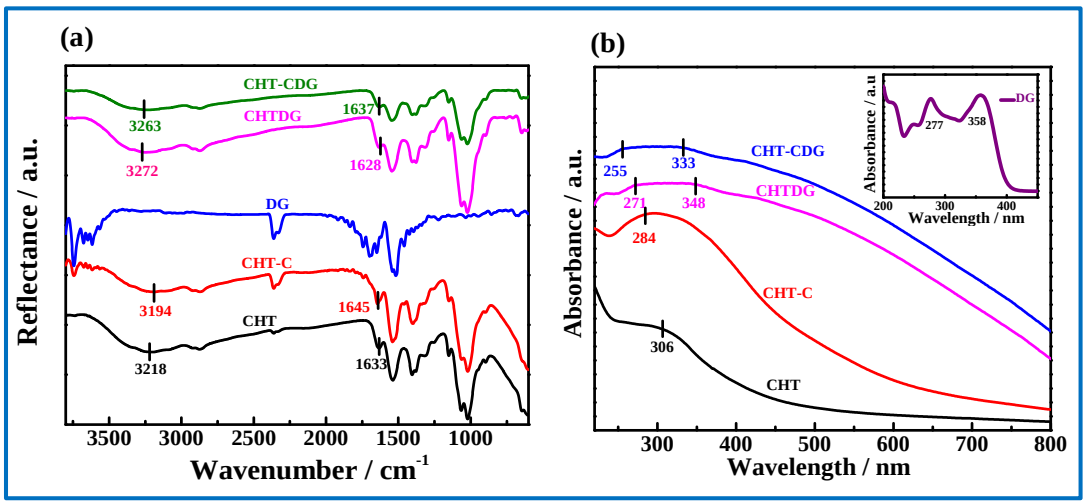

Figure 5.6: (a) FTIR spectra of drug encapsulated CHT matrix and its indicated nanohybrids, where DG represents the pure drug and DG after sample coding indicates corresponding drug loaded sample. (b) UV-visible spectra of drug embedded pure CHT and its indicated nanohybrids. Inset figure represents the UV-visible Spectra of pure drug is shown in inset figure.

embedded samples. The shifting is found to be greater in nanohybrid. The FTIR and UV-visible measurements reveal that drug molecules interact with the matrix greater way in

nanohybrid as compared to pure chitosan which is well reflected in drug release pattern showing slow drug release in nanohybrids. Moreover, nanoparticles in the matrix increase the barrier properties creating a maze which slow down the diffusion process of the drug molecules from the matrix resulting in slower drug release kinetics. The slower release kinetics in nanohybrids as compared to the pure chitosan is mainly responsible for greater interaction of the drug molecules with nanohybrids and the barrier effect of nanoparticles. A schematic model has been proposed comparing the fast and slow release of drug from pure CHT and their corresponding nanohybrid (**Figure 5.5c**).

The developed nanohybrids (hydrogel and scaffold) are very promising candidate for sustained drug delivery and the release rate can be tuned with the suitable choice of nanoparticles.

5.2.4 Biocompatibility Test

Hydrogel and scaffold of nanohybrids with sufficient mechanical stability are the promising candidate to be used as drug delivery vehicles in biomedical application. Therefore, cytotoxicity of the hydrogel and scaffold of pure chitosan and its nanohybrids is an essential criterion before using them as drug delivery systems. Cytotoxicity is investigated by MTT assay through cell growth of 3T3 cells on the surface of the hydrogels and scaffolds. The viability of cells on hydrogel and scaffolds are shown in **Figure 5.7a&b**, respectively. It is clearly observed from the cell viability test that the numbers of viable cells are gradually increased showing the well biocompatibility of the hydrogel and scaffolds of nanohybrids. It is interesting to note that viability of the cells on the scaffold is greater than that on hydrogel, which indicates scaffolds are more biocompatibile in nature than hydrogel. Fluorescence images of proliferated cells on

hydrogel and scaffold also confirms the MTT assay showing a greater number of cell density in nanohybrids as compared to the pure chitosan (**Figure 5.7c&d**).

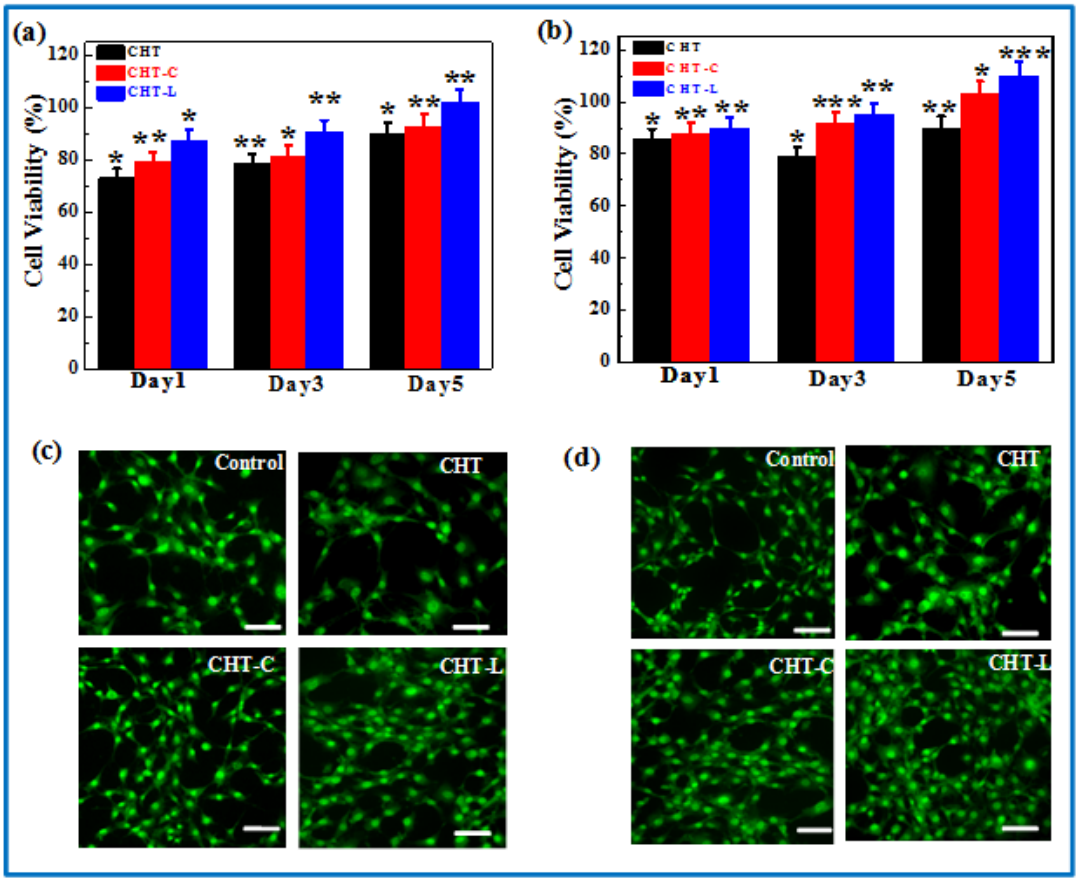

Figure 5.7: Cell viability assay of pure CHT and its corresponding nanohybrids after predetermined time using (a) hydrogel and (b) Scaffold; All the data presented here are mean ± standard deviation values obtained from three independent experiments, where *P<0.05, **P<0.01 and ***P<0.0001. Fluorescence images of the proliferated cells after five day on hydrogel (c) and scaffold (d); scale bar = 45 µm.

Furthermore, among the nanohybrids, LDH based chitosan nanocomposite (CHT-L) are more biocompatible in nature than nanoclay based one (CHT-C) in both cases (hydrogel and scaffold).

To study the proliferation of cells within the scaffold, cell seeded scaffolds are observed in SEM (**Figure 5.8**). Cells proliferation nature in pristine chitosan and its corresponding nanohybrids is quite different. After completion of the 5 days of culture,

cell clusters are observed on the surface of the chitosan scaffold, while cell clusters are observed inside of the pores of the nanohybrid scaffold. Nanohybrids with high mechanical strength with less collapsible pore structure promote the cell growth and proliferation inside the pores and pore a wall which is very essential criteria for tissue engineering purposes.

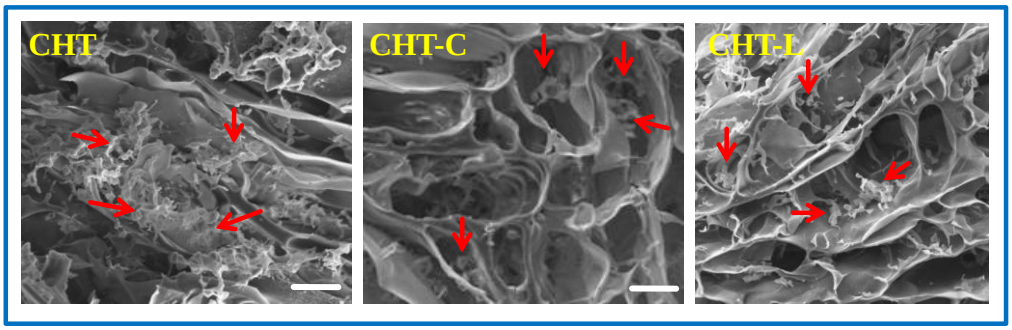

Figure 5.8: SEM images of the cell seeded scaffold of pure CHT and its indicated nanohybrid. Red arrow indicates actual the position of the cells on scaffolds. Scale bar = 60 µm.

5.3 Conclusion

A new type of chitosan hydrogels and scaffolds have been developed using two different types of nanofillers (30B and LDH). Homogeneous dispersion of the nanofillers in the polymer matrix significantly enhance the different physicochemical properties of the pure chitosan. The morphological investigation of nanohybrids hydrogel shows a porous network structure. Phase diagram (Temperature vs. Concentration) reveals that using LDH as a nanofiller working window of chitosan hydrogel can be increased. The dramatic enhancement of the mechanical strength of nanohybrids (hydrogel and scaffolds) as compared to pristine polymer is observed as a consequence of the extensive interaction between nanofillers and the pure polymer. The sufficient mechanical strength of the nanohybrids makes them suitable for biomedical application. The tunable sustained drug release behavior of the nanohybrids is achieved using drug embedded hydrogel and

scaffolds as compared to the pure chitosan. Biocompatibility test has been carried out through the MTT assay with NIH 3T3 cell. Nanohybrids are found to be nontoxic in nature and better biocompatible than pure chitosan. Henceforth, nanohybrids hydrogel and scaffold are suitable biomaterials for future biomedical applications.